Supporting Information

Isolated Single Iron Atoms Anchored on N, S-Codoped Hierarchically Ordered Porous Carbon Framework for Highly Efficient Oxygen Reduction

*Xinghuan Liu[+], Xingwu Zhai[+], Wenbo Sheng, Juan Tu, Zeyu Zhao, Yulin Shi, Caixia Xu, Guixian Ge, Xin Jia**

X. Liu[+], X. Zhai[+], W. Sheng, J. Tu, Z. Zhao, Prof. Shi, Prof. C. Xu, Prof. X. Jia
School of Chemistry and Chemical Engineering/Key Laboratory for Green Processing of Chemical Engineering of Xinjiang Bingtuan, Key Laboratory of Materials-Oriented Chemical Engineering of Xinjiang Uygur Autonomous Region, Engineering Research Center of Materials-Oriented Chemical Engineering of Xinjiang Bingtuan, Shihezi University, Shihezi 832003, China.
E-mail: jiaxin@shzu.edu.cn
Prof. G. Ge
Key Laboratory of Ecophysics and Department of Physics, College of Science, Shihezi University, Shihezi, 832003, PR China, Email: geguixian@126.com
[+] These authors contributed equally to this work.

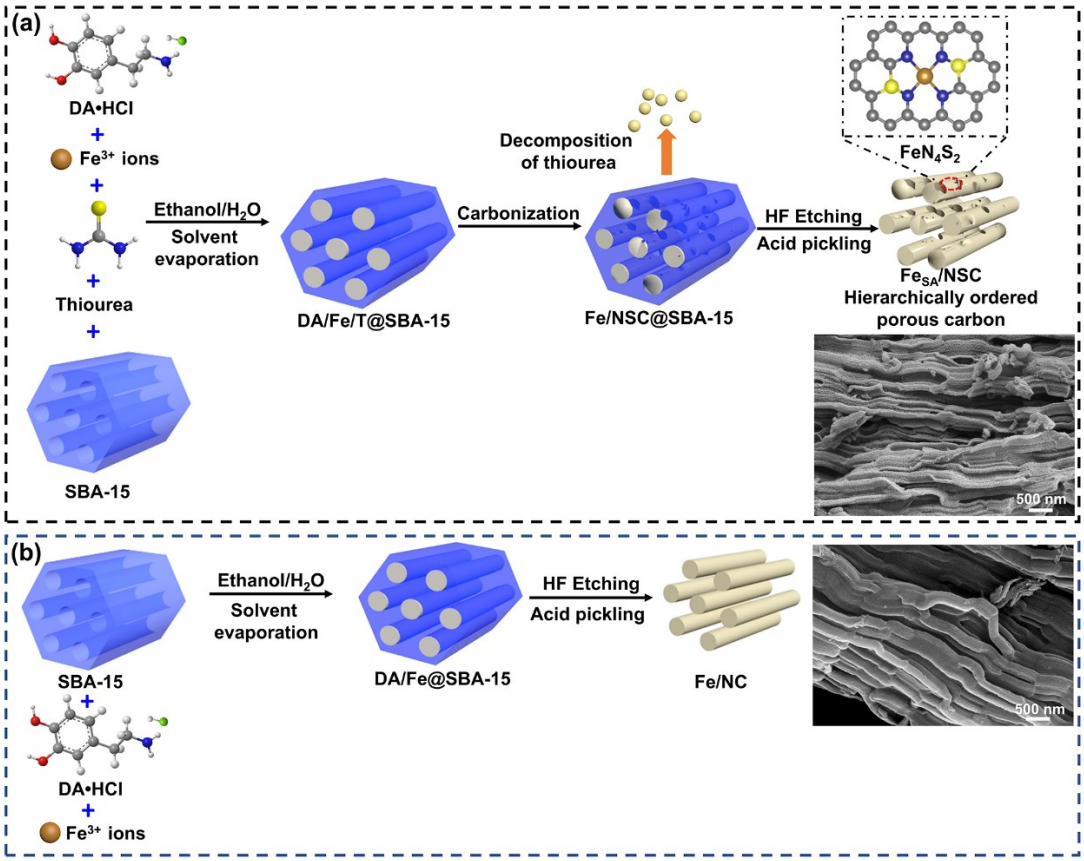

Scheme S1 (a) Synthetic route of Fe_{SA}/NSC hierarchically ordered porous carbon (HOPC) materials. (b) General synthetic route of ordered mesoporous carbon (OMC) materials.

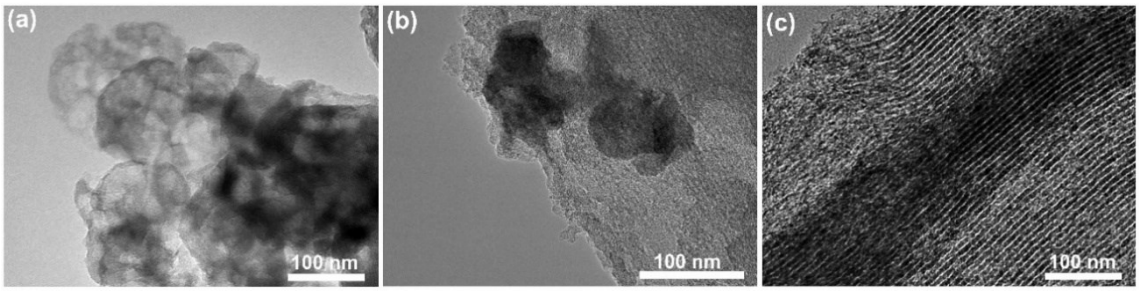

Figure S1 (a) and (b) TEM images of the carbon materials obtained by solvent evaporation process using polydopamine/Fe as precursor; (c) TEM images of the carbon materials prepared solvent evaporation method using dopamine/Fe as precursor.

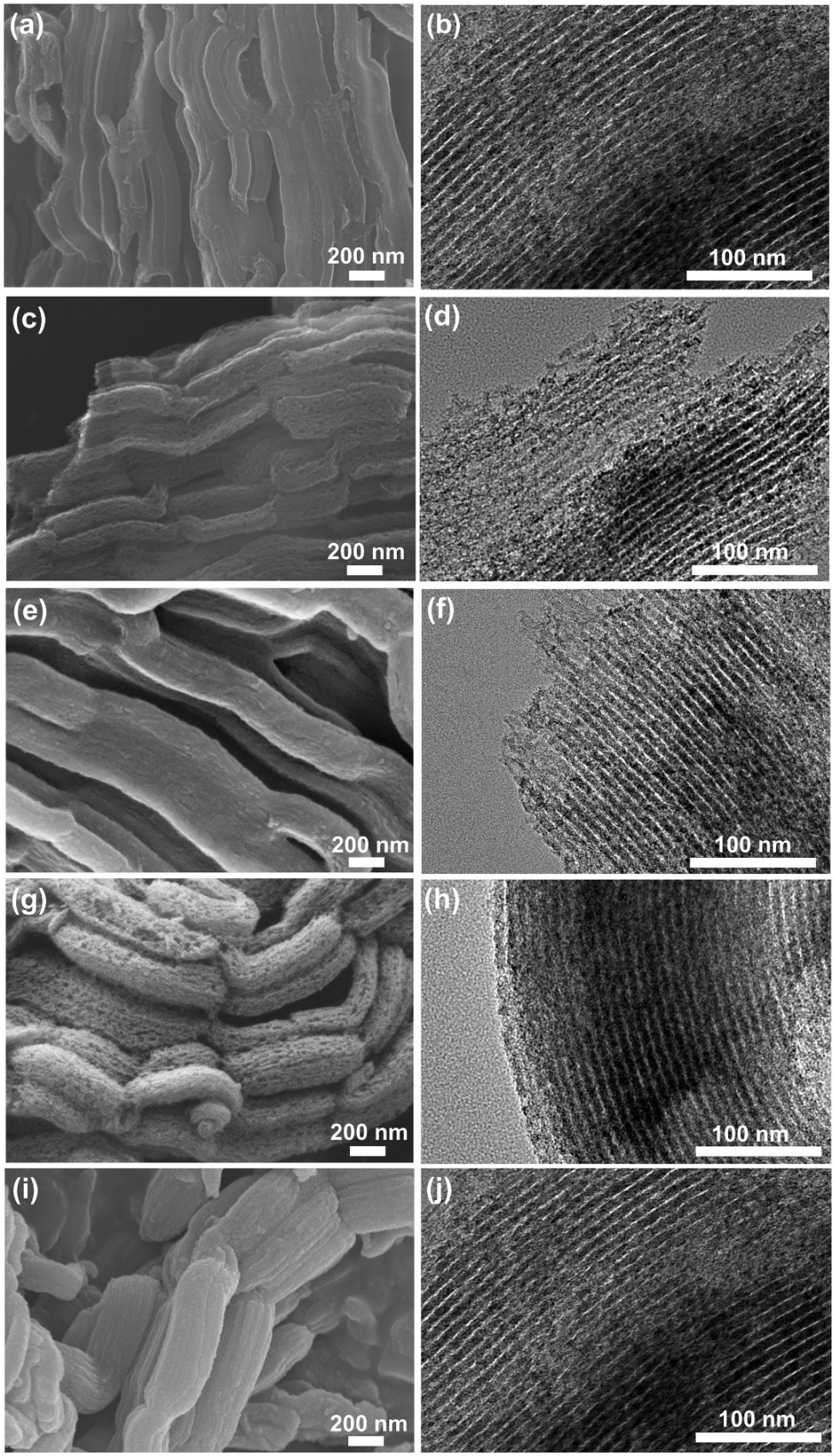

Figure S2 SEM images of (a) Fe/NSC-TO, (c) Fe/NC-UI, (e) Fe/NC, (g) NSC, (i) NC. TEM images of (b) Fe/NSC-TO, (d) Fe/NC-UI, (f) Fe/NC, (h) NSC, (j) NC.

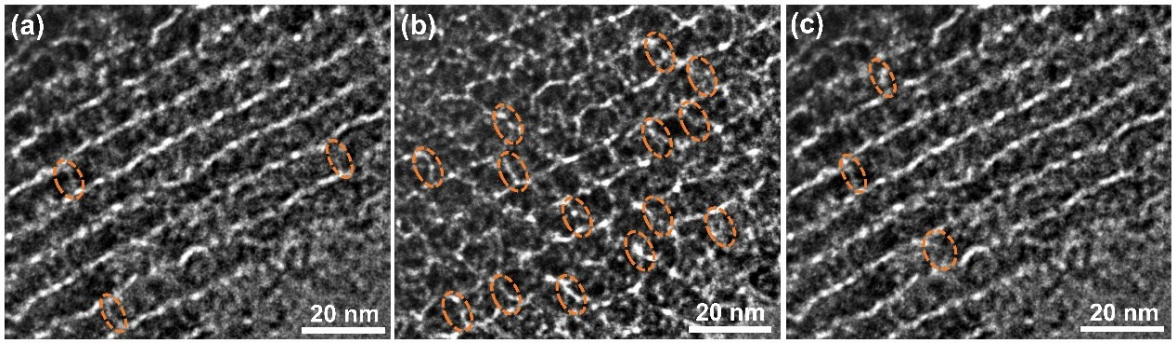

Figure S3 HRTEM images of (a) Fe/NSC-TO, (b) Fe/NC-UI, (c) Fe/NC. Some obvious micropore and mesoporous structures are highlights by saffron yellow circles.

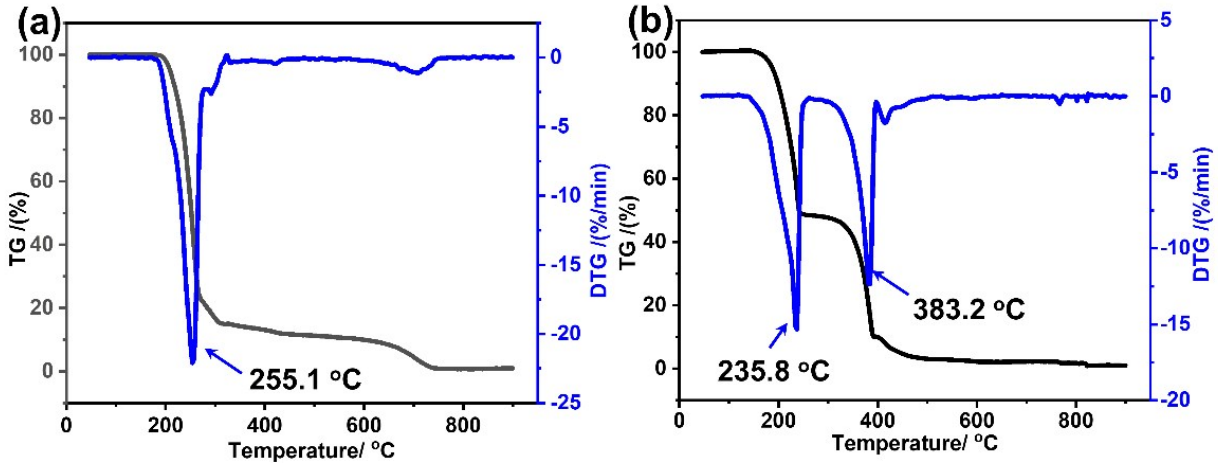

Figure S4 Thermogravimetric analyses of (a) thiourea and (b) urea.

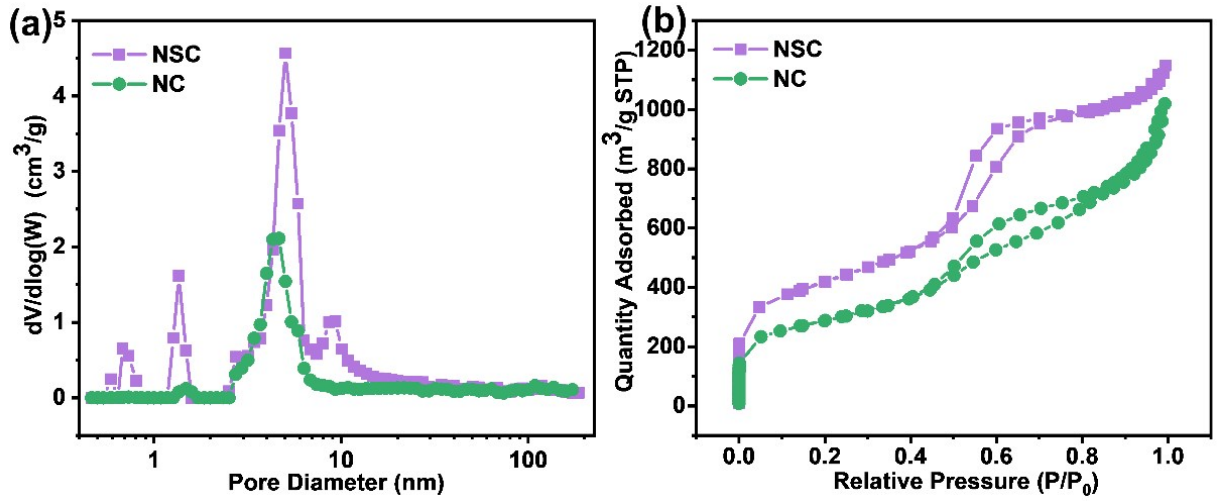

Figure S5 (a) Nitrogen adsorption–desorption isotherms spectra and (b) pore size distribution (PSD) curves of NSC and NC, respectively.

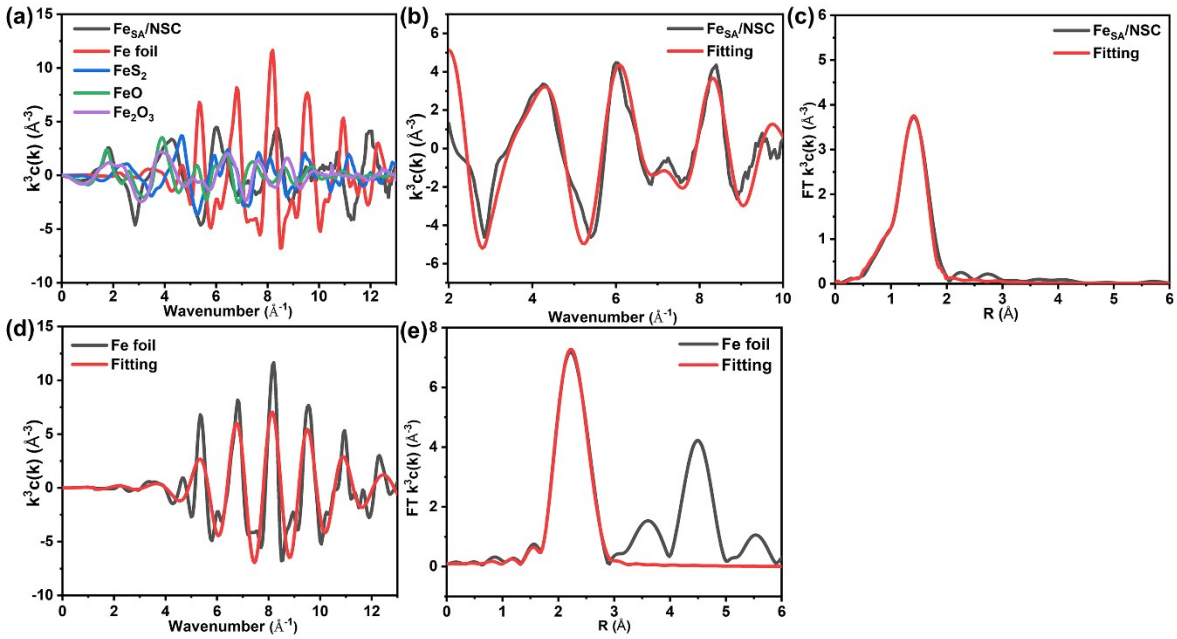

Figure S6 (a) The *k3*-weighted EXAFS in *K*-space for Fe_{SA}/NSC, Fe foil, FeS_2, FeO and Fe_2O_3, (b) Fe *K*-space (c) FT-EXAFS fitting curves of the Fe_{SA}/NSC at Fe K-edge. (d) Fe *K*-space (e) FT-EXAFS fitting curves of the Fe-foil at Fe K-edge.

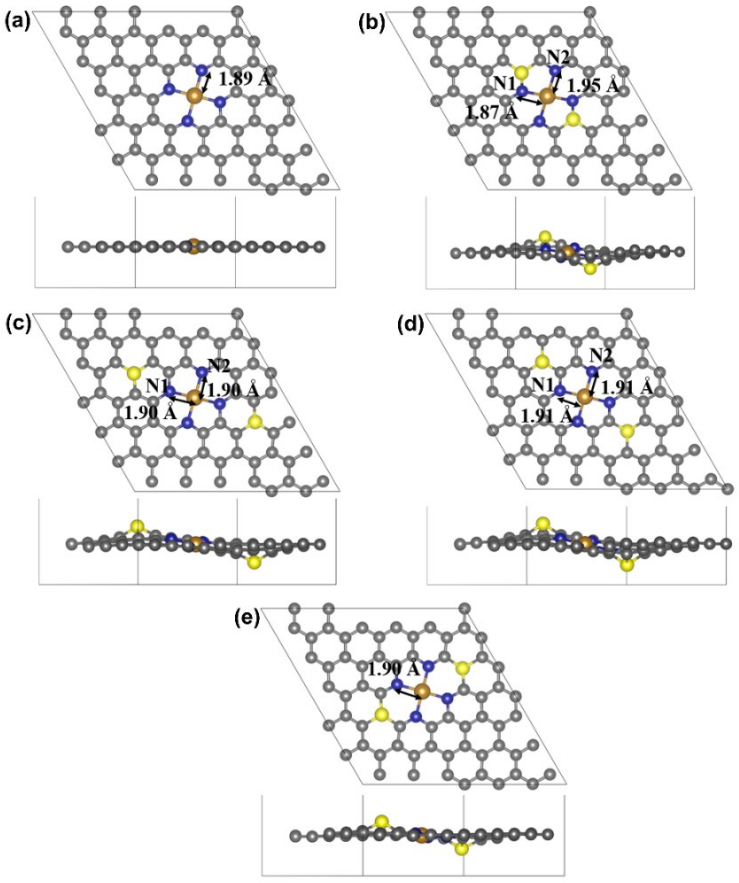

Figure S7 (a) Top and side view of FeN_4 model. (b-e) Optimized geometries of four types possible FeN_4S_2 active site structure. Fe-N bond lengths are also presented. Corresponding element: S (yellow), N (blue), Fe (gold), C (gray).

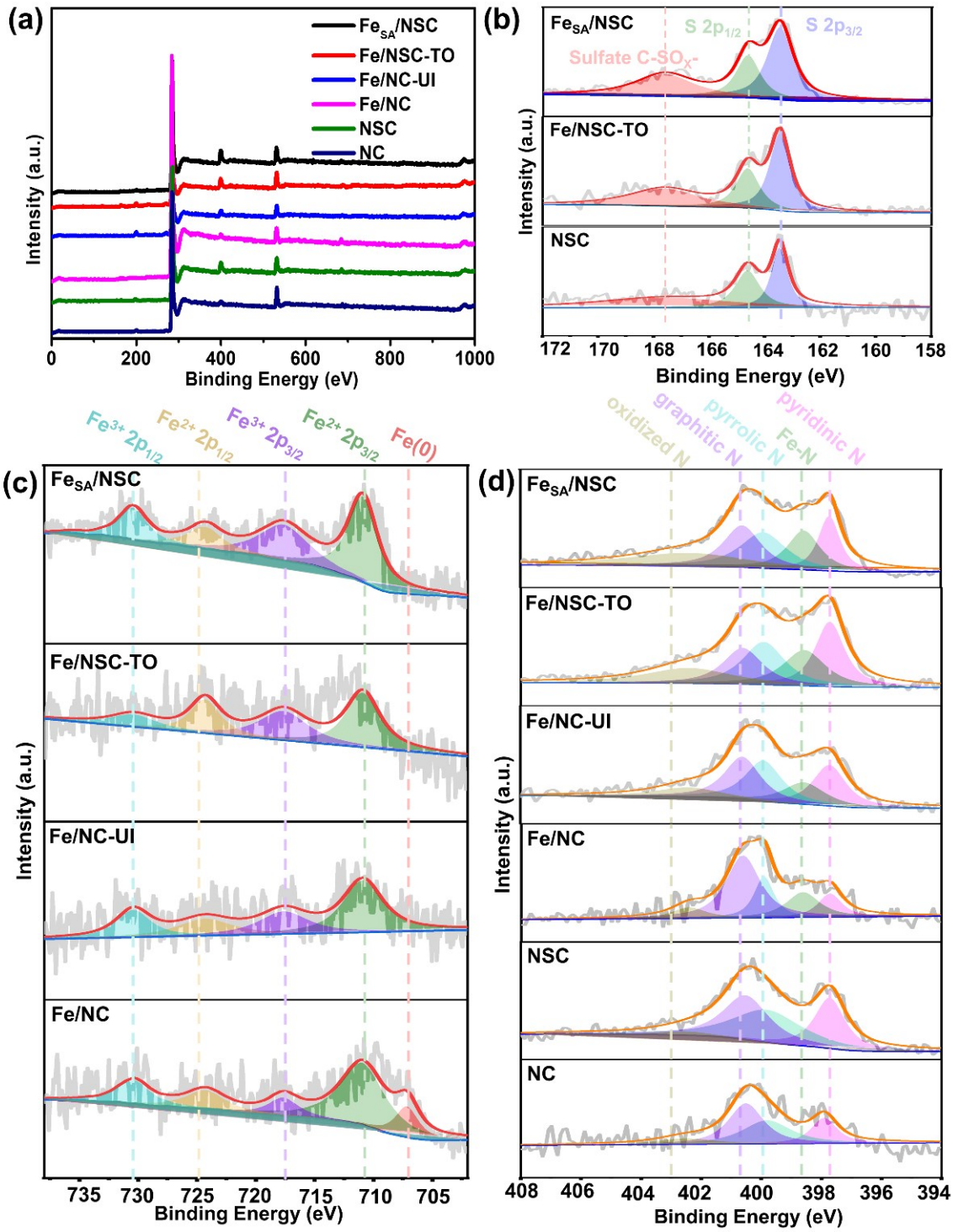

Figure S8 (a) The wide-range XPS spectra of catalysts; (b) The high-resolution S 2p spectra of Fe_{SA}/NSC, Fe/NSC-TO and NSC. (c) The high-resolution Fe 2p XPS spectrum of Fe_{SA}/NSC, Fe/NSC-TO, Fe/NC-UI, Fe/NC. (d) The high-resolution N 1s spectra of Fe_{SA}/NSC, Fe/NSC-TO, Fe/NC-UI, Fe/NC, NSC, NC

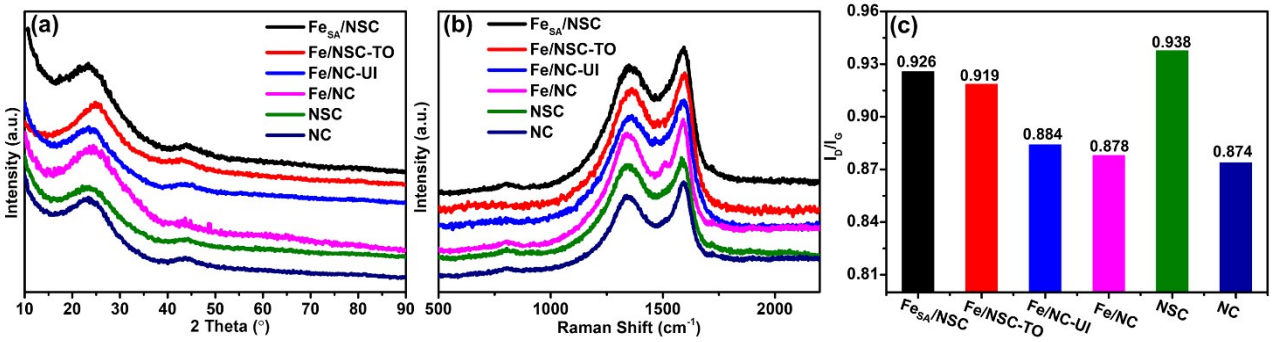

Figure S9 (a) XRD, (b) Raman spectra and (c) I_D/I_G radio of Fe_{SA}/NSC, Fe/NSC-TO, Fe/NC-UI, Fe/NC, NSC and NC, respectively.

As shown in Figure S9b, the corresponding Raman spectra showed obvious characteristic D and G bands at about 1350 cm^{-1} and 1589 cm^{-1}, which are assigned to sp^3 defective sites and sp^2-hybridized graphitic carbon atoms, respectively. Figure S9c showed that the ratio of I_D/I_G of the Fe_{SA}/NSC (0.926) is larger than those of Fe/NSC-TO (0.919), Fe/NC-UI (0.884) and Fe/NC (0.878). The possible reseason is the enrichment of structural defects after the doping of S and the forming of HOPC structures.

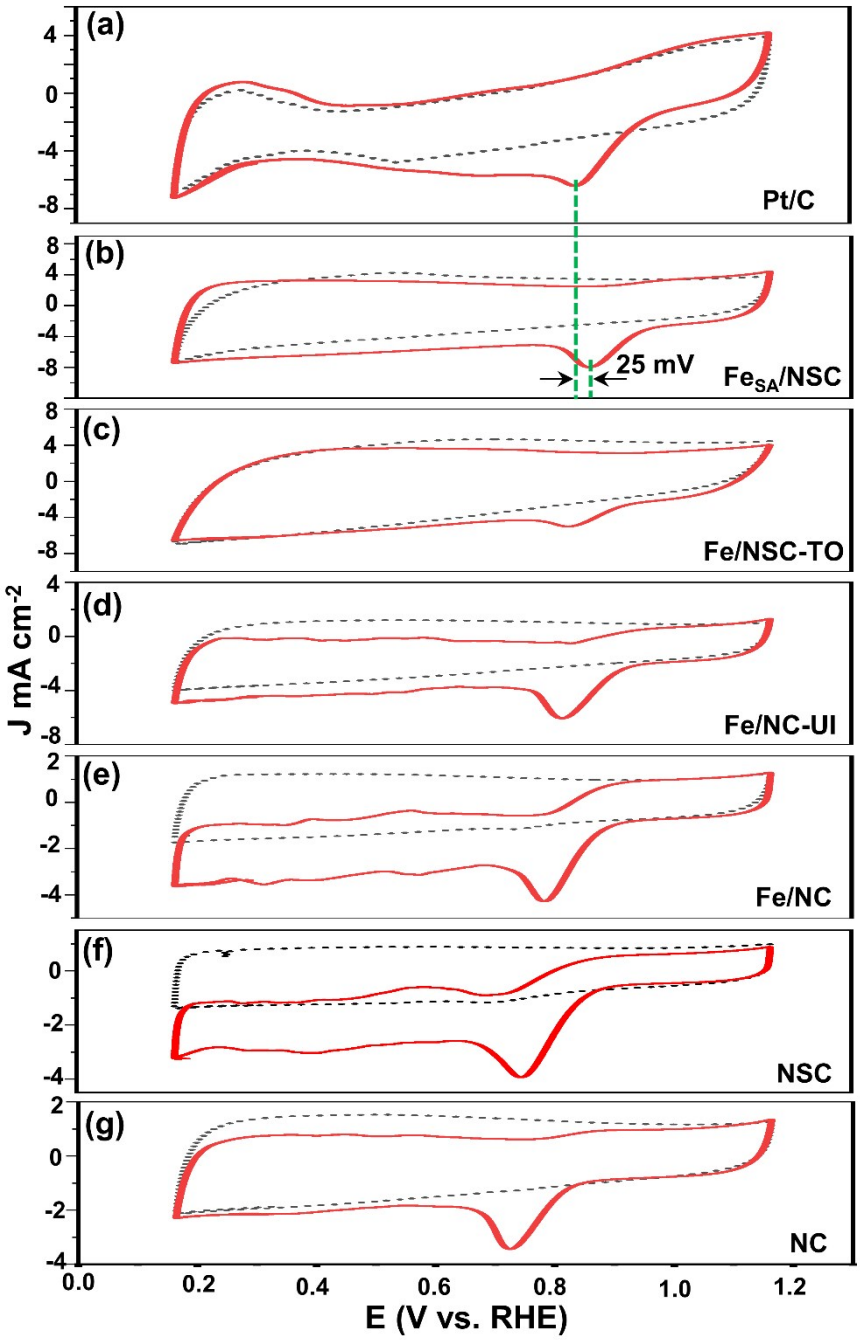

Figure S10 Cyclic voltammetry curves of different catalysts in N_2- (black dotted line) and O_2- (red line) saturated 0.1 M KOH solution at a scan rate of 50 mV s^{-1}: (a) Pt/C, (b) Fe_{SA}/NSC, (c) Fe/NSC-TO, (d) Fe/NC-UI, (e) Fe/NC, (f) NSC, (g) NC.

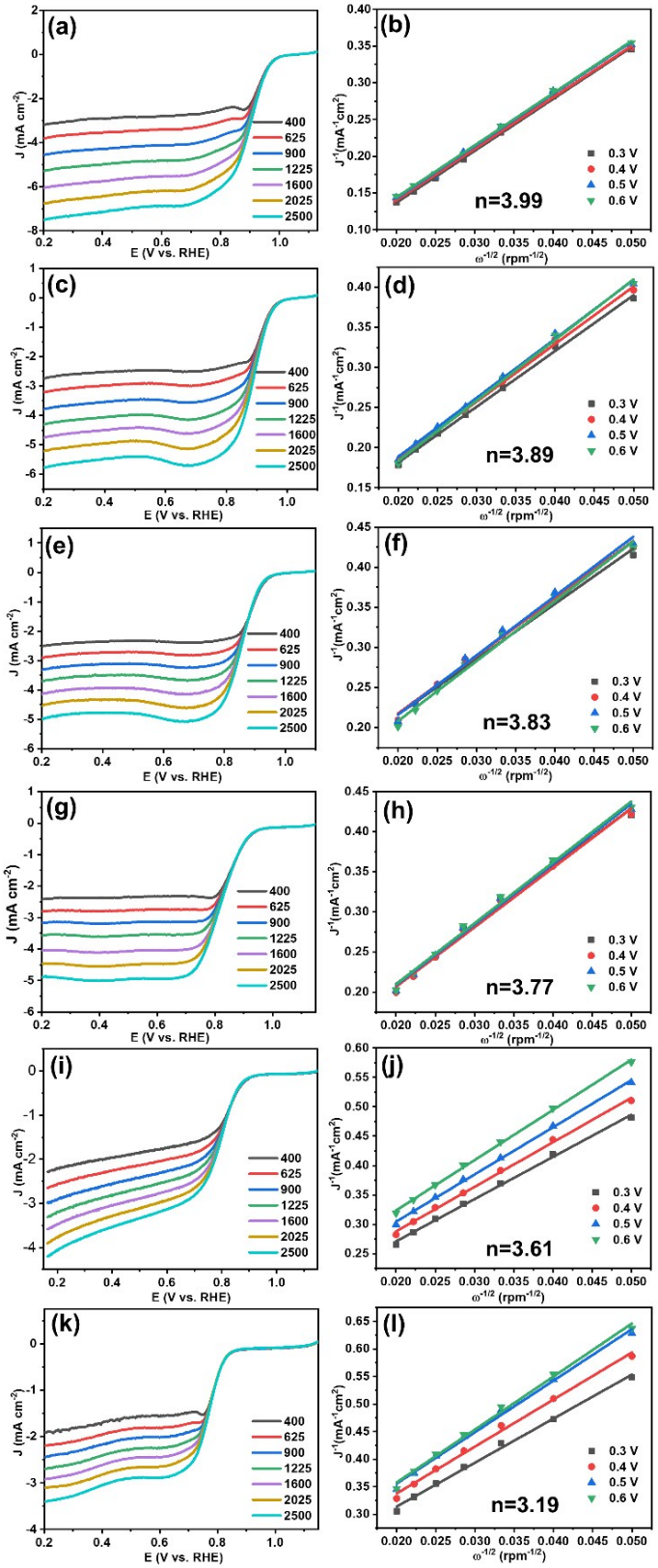

Figure S11 LSV curves of (a) Fe_{SA}/NSC, (c) Fe/NSC-TE, (e) Fe/NC-UI, (g) Fe/NC, (i) NSC, (k) NC at different rotating speeds in 0.1 M KOH, respectively. The corresponding K-L plots at different potentials: (b) Fe_{SA}/NSC, (d) Fe/NSC-TO, (f) Fe/NC-UI, (h) Fe/NC, (j) NSC, (l) NC.

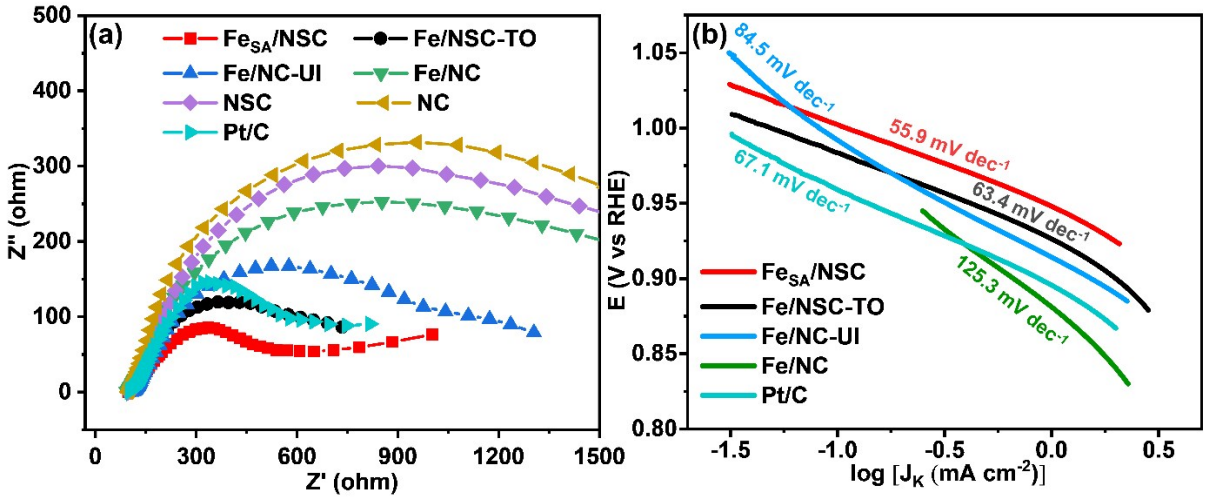

Figure S12 (a) The electrochemical impedance spectrum of Fe_{SA}/NSC, Fe/NSC-TO, Fe/NC-UI, Fe/NC, NSC, NC and Pt/C. (b) Tafel slopes of Fe_{SA}/NSC, Fe/NSC-TO, Fe/NC-UI, Fe/NC and Pt/C catalysts.

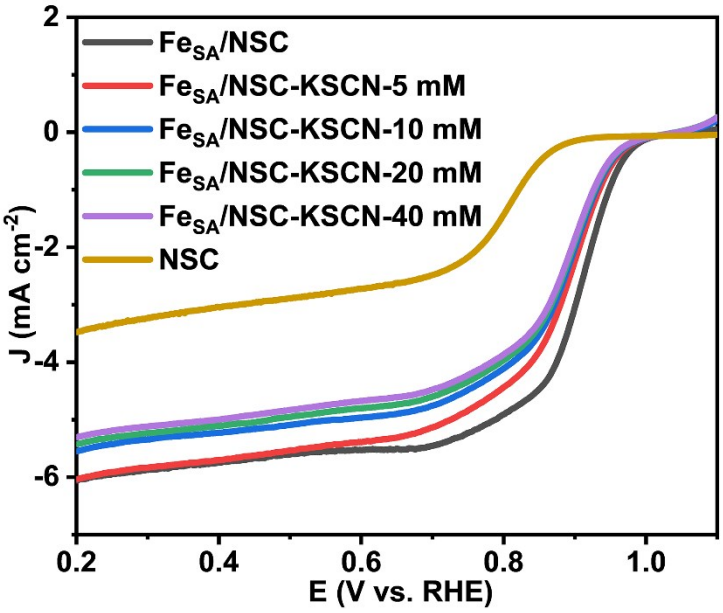

Figure S13 Steady-state ORR polarization curves of Fe_{SA}/NSC recorded in O_2 saturated 0.1 M KOH, ORR polarization curves of Fe_{SA}/NSC poisoning by 5 mM 10 mM, 20 mM and 40 mM SCN^- and the ORR polarization curves of NSC.

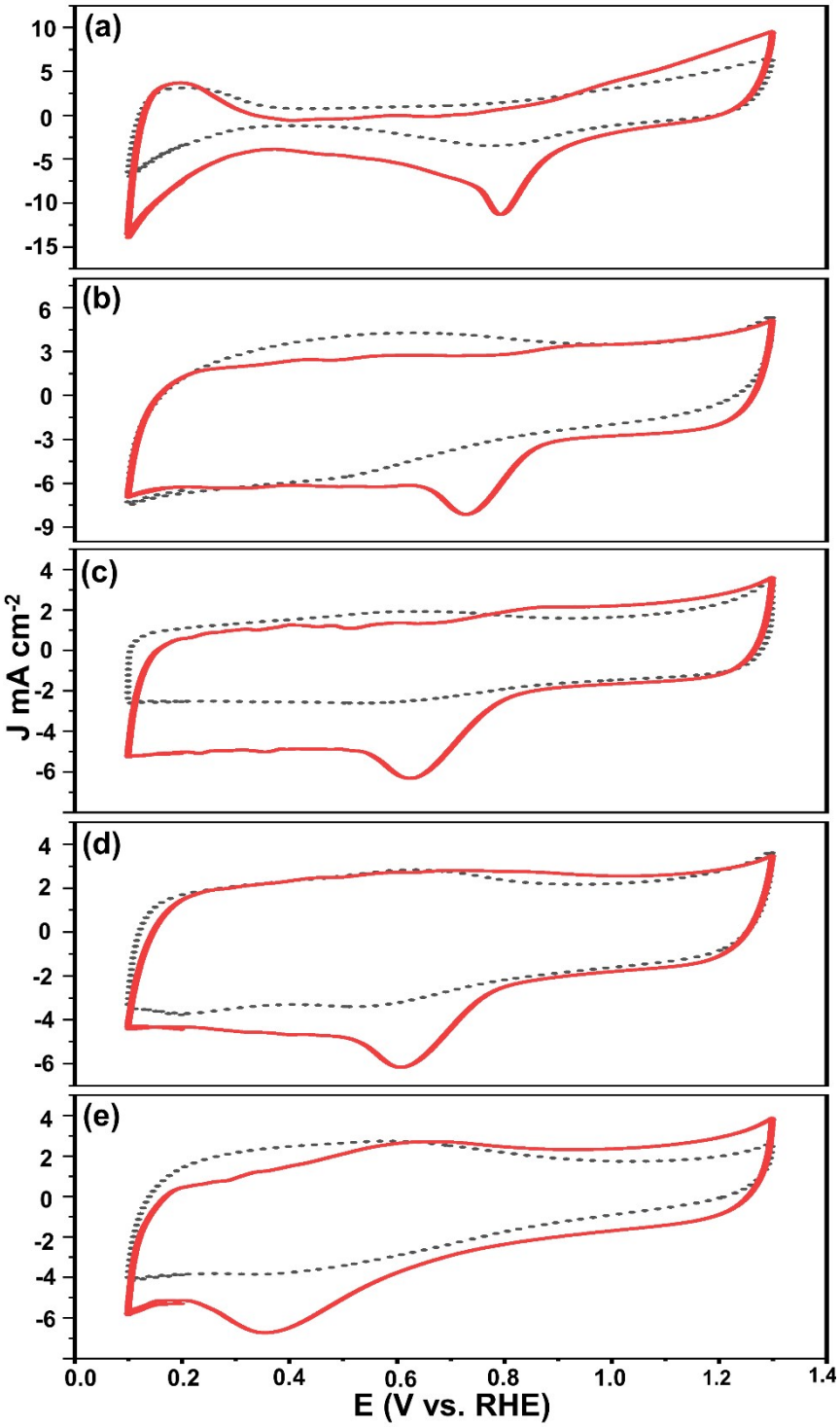

Figure S14 Cyclic voltammetry curves of different catalysts in N_2- (black dotted line) and O_2- (red line) saturated 0.1 M $HClO_4$ solution with a scan rate of 50 mV s^{-1}: (a) Pt/C, (b) Fe_{SA}/NSC, (c) Fe/NSC-TO, (d) Fe/NC-UI and (e) Fe/NC.

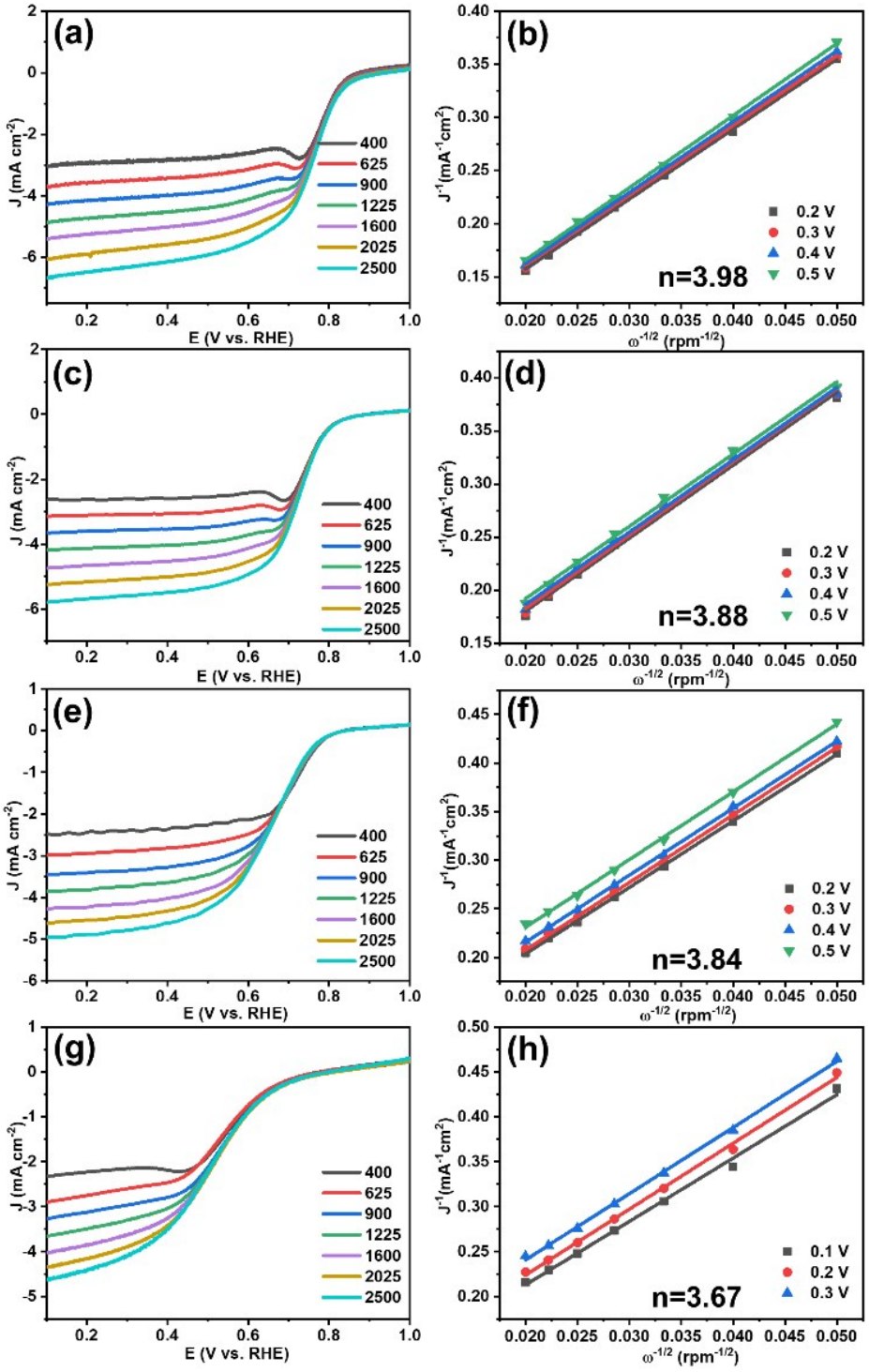

Figure S15 LSV curves of (a) Fe_{SA}/NSC, (c) Fe/NSC-TO, (e) Fe/NC-UI and (g) Fe/NC at different rotating speeds in 0.1 M $HClO_4$ solution, respectively. The corresponding K-L plots at different potentials, (b) Fe_{SA}/NSC, (d) Fe/NSC-TO, (f) Fe/NC-UI and (h) Fe/NC, respectively.

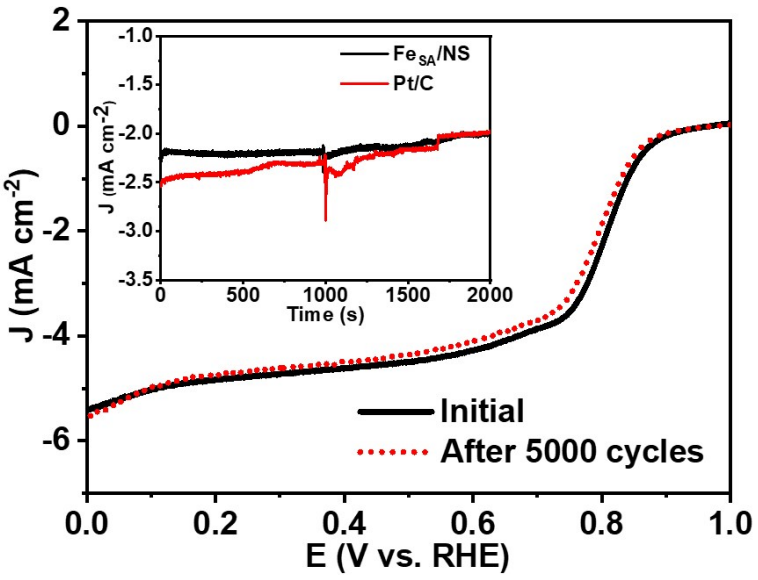

Figure S16 Stability test of Fe_{SA}/NSC (inset: chronoamperometric curves of a methanol crossover test at 0.5 V before and after adding of 0.5 M methanol) in 0.1 M $HClO_4$

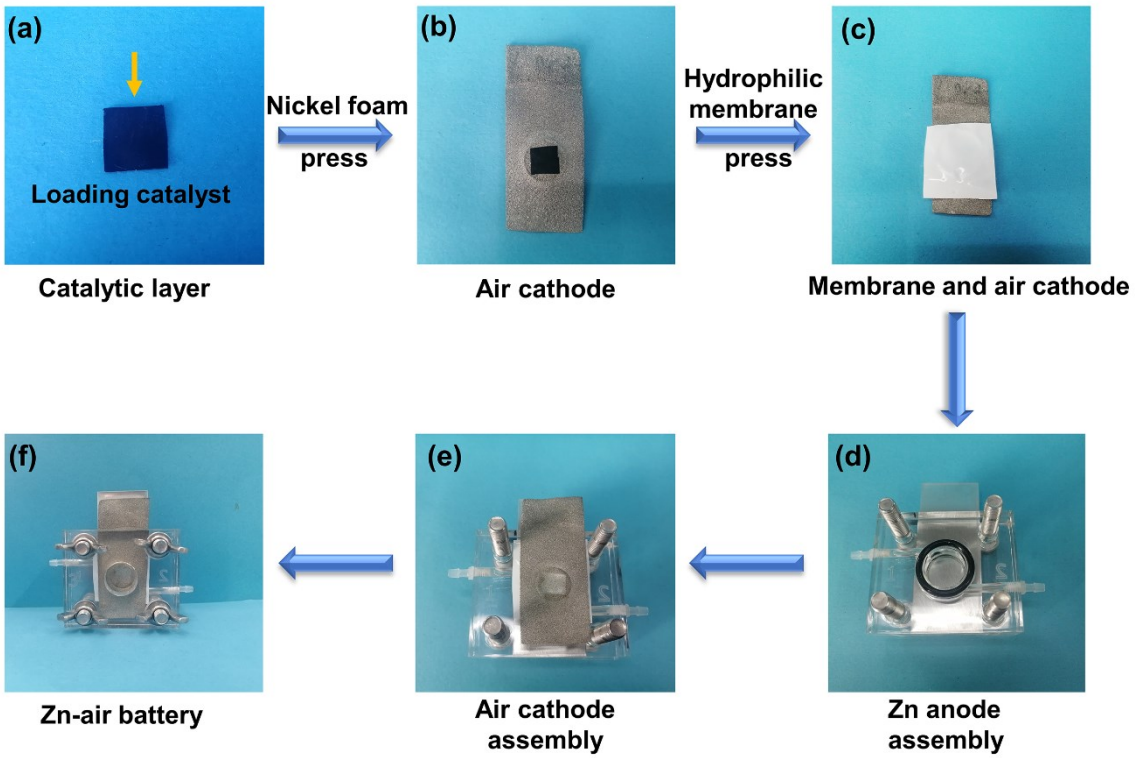

Figure S17 Photographs of the assembly process of Zn-air battery: (a) catalytic layer, (b) air cathode, (c) hydrophilic membrane and air cathode, (d) Zn anode assembly, (e) air cathode assembly, (f) Zn-air battery.

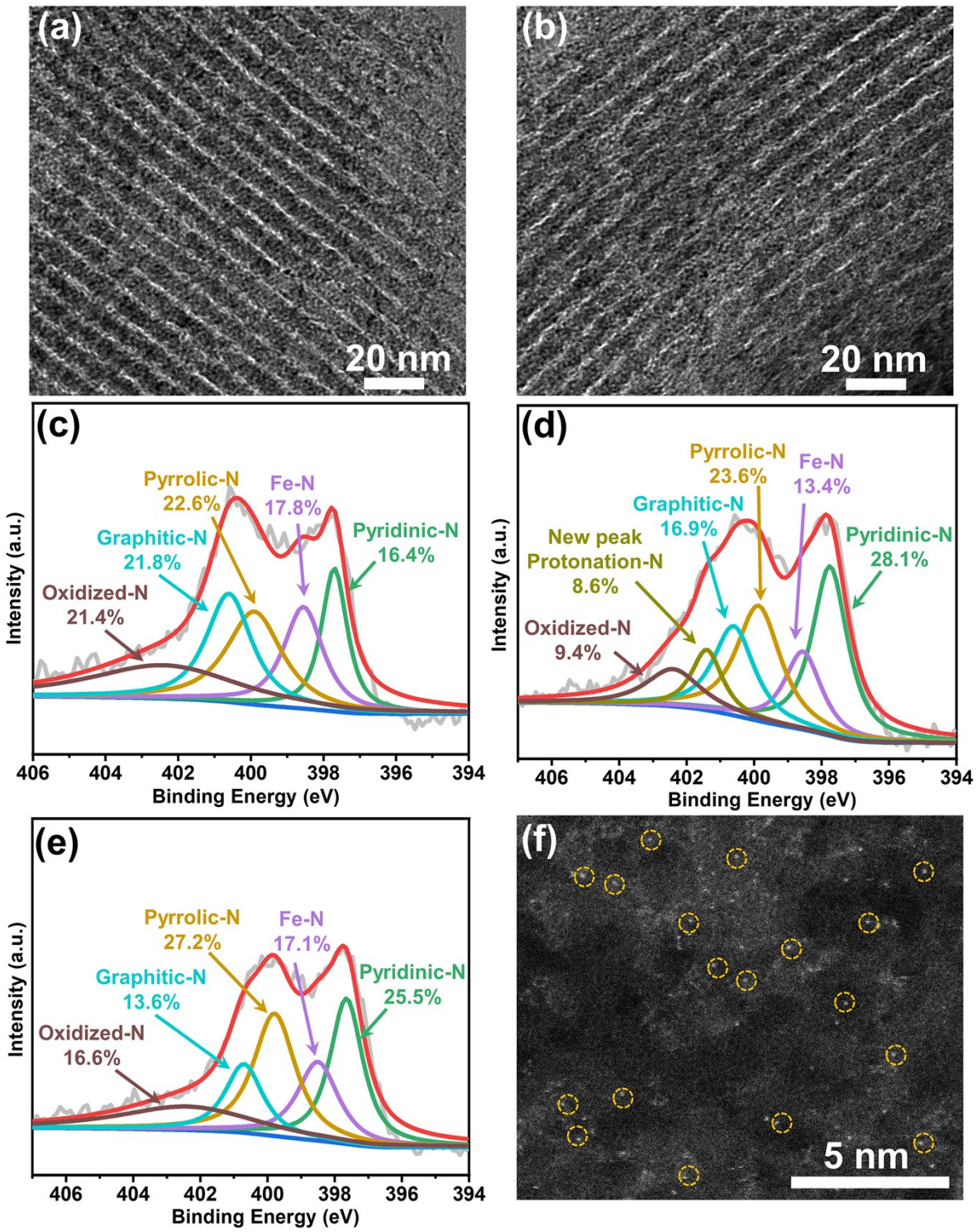

Figure S18 HRTEM images of Fe_{SA}/NSC after 5000 cycles between 0.8 and 1.1 V versus RHE in (a) 0.1 M KOH and (b) 0.1 M $HClO_4$ solutions. High-resolution of N1s spectra of Fe_{SA}/NSC (c) before and after 5000 cycles in (e) 0.1 M KOH and (d) 0.1 M $HClO_4$ solutions.

(f) High-resolution HAADF-STEM images of the Fe_{SA}/NSC after stability test in acidic electrolyte.

As shown in Figure S18a and b, the Fe_{SA}/NSC still maintained the original ordered porous structures, and no metal agglomeration was observed after 5000 cycles in 0.1 M KOH and 0.1 M $HClO_4$ solutions. In addition, to deeply understand the origin of the stability in both alkaline and acidic media, XPS measurements were adopted to measure the changes of N types. High-resolution N1s spectra of original Fe_{SA}/NSC can be fitted into five peaks, pyridinic N at 397.8 eV, Fe-N at 398.6 eV, pyrrolic N at 399.9 eV, graphitic N at 400.7 eV and oxidized N at 402.4 eV. In this paper, the catalytic center of Fe_{SA}/NSC is Fe-N relative sites. Thus, we focus on the changes of Fe-N peaks. After 5000 CV cycles in alkaline solutions, the contents of Fe-N exhibits a relatively small decrease (from 17.8% to 17.1% in Figure S18c and e). After stability measurement, a new peak associated with the protonation of pyridinic-N was observed at around 401.4 eV (protonation-N)[1]. Moreover, we found that the contents of the Fe-N shows a decrease from 17.8% to 13.4%. This may be one of the reason why the stablity of the Fe_{SA}/NSC in alkaline media is better than that of acid media. Moreover, considering that the obvious decrease of the Fe-N content after stability test in acid media, We used HAADF-STEM to monitor the dispersed state of the Fe species, which displays that Fe species were still atomically dispersed on the carbon support (marked with yellow circles) after stability test in acid media.

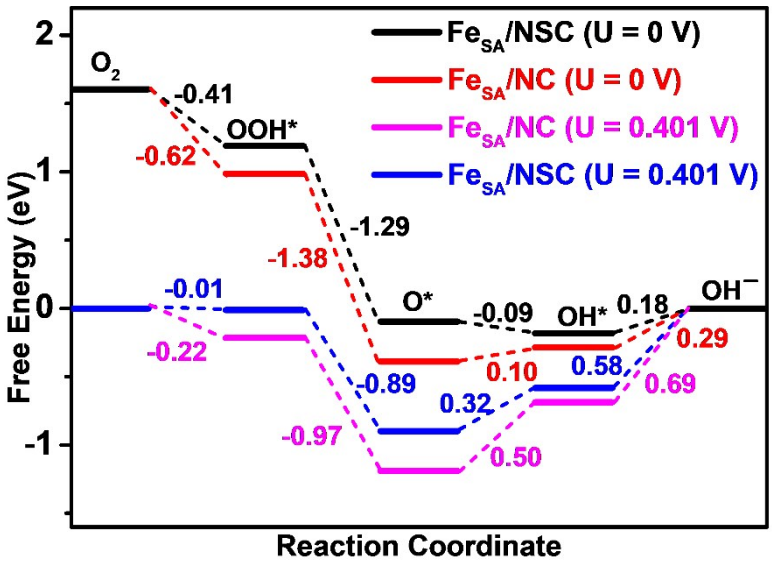

Figure S19 The Gibbs free energy diagram of ORR on Fe_{SA}/NSC and Fe_{SA}/NC under alkaline condition by DFT calculations.

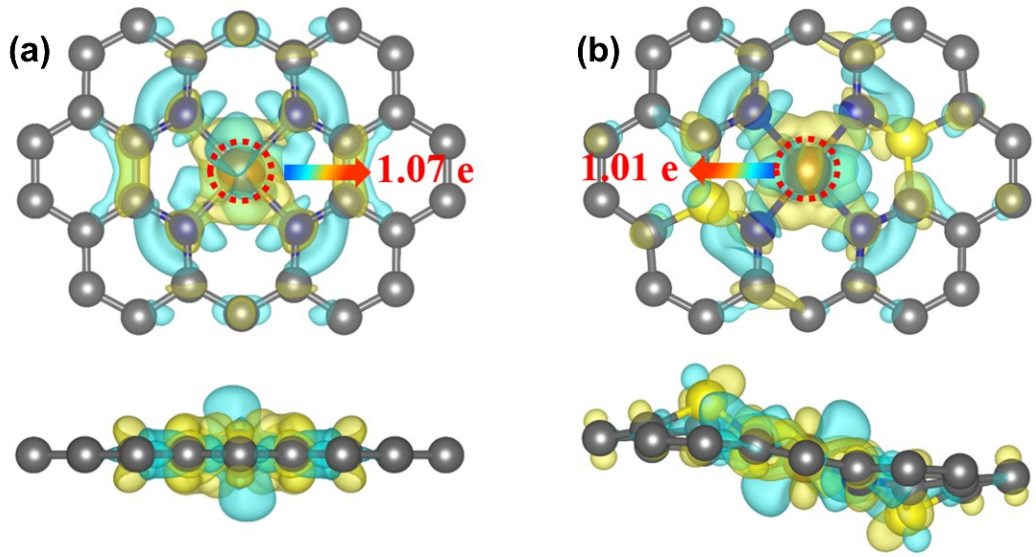

Figure S20 Top and side views of the charge density difference and Bader charge analysis for (a) Fe_{SA}/NC and (b) Fe_{SA}/NSC. The isosurface level is 0.003 e/Å^3. Yellow and cyan areas represent electron accumulation and depletion regions.

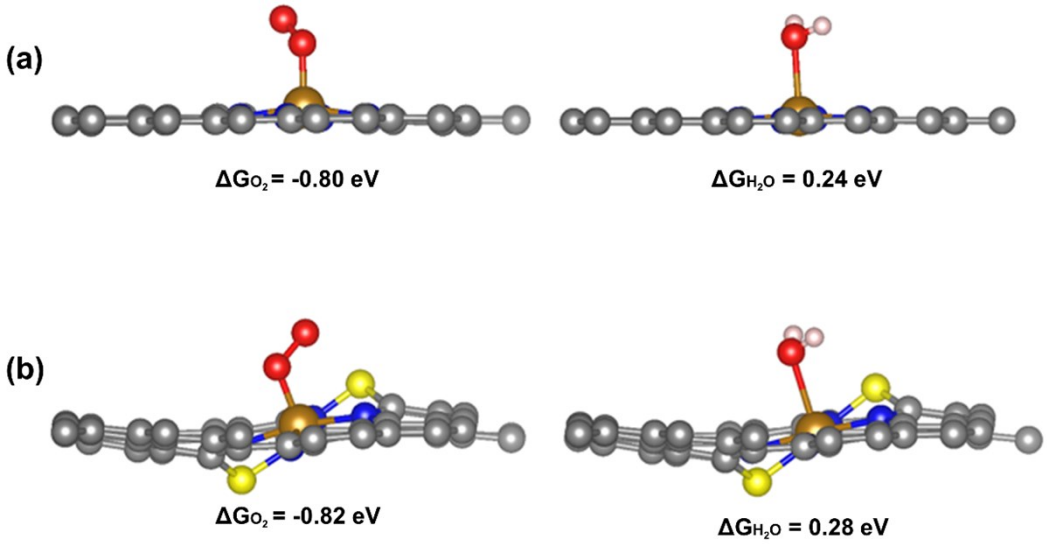

Figure S21 Adsorption free energy of O_2 or H_2O on (a) Fe_{SA}/NSC and (b) Fe_{SA}/NC.

Table S1 Bond lengths of O_2 molecules, $O_{next\text{-}nearest}$-Fe, $O_{nearest}$-Fe, H_2O-Fe on Fe_{SA}/NSC and Fe_{SA}/NC from Figure S21

	Fe_{SA}/NC (Å)	Fe_{SA}/NSC (Å)
O-O	1.299	1.313
$O_{next\text{-}nearest}$-Fe	2.773	2.631
$O_{nearest}$-Fe	1.815	1.792
H_2O-Fe	2.362	2.405

As shown in Figure S21, O_2 molecule is adsorbed on the Fe_{SA}/NSC site in the end-on model with a adsorption free energy (ΔG_{O_2}) of -0.82 eV, which is lower than that on the Fe_{SA}/NC site

(-0.80 eV). On the contrary, the adsorption free energy of H_2O on the Fe_{SA}/NSC and Fe_{SA}/NC sites was 0.28 eV and 0.24 eV, respectively. The results indicats that Fe_{SA}/NSC could bind O_2 more efficiently to initiate the ORR and bind H_2O weakly to complete the reaction. In addition, the bond lengths (1.313 Å) of O_2 molecules adsorbed on the surface of Fe_{SA}/NSC is longer than that of Fe_{SA}/NC (1.299 Å), which shows that Fe_{SA}/NSC can activate O_2 molecules favorably. At the same time, for Fe_{SA}/NC and Fe_{SA}/NSC systems, the bond lengths of $O_{nearest}$-Fe is basically the same. The bond length of $O_{next\text{-}nearest}$-Fe (2.773 Å) in Fe_{SA}/NC is greater than that of Fe_{SA}/NSC (2.631 Å), indicating that the difference in O_2 adsorption energy is mainly due to the difference in $O_{next\text{-}nearest}$-Fe bond lengths. Furthermore, the bond length of H_2O-Fe (2.405 Å) in Fe-SAs/NSC is greater than that in Fe_{SA}/NC (2.362 Å), indicating favorable desorption of H_2O.

Table S2 EXAFS fitting parameters at the Fe K-edge for various samples（S_0^2=0.85）

Sample	Bond type	N1	R(Å)	$\sigma^2 \times 10^{-3}$ (Å^2)	ΔE_0 (eV)	R factor
Fe_{SA}/NSC	Fe-N1	1.9	1.98	8.2	2.9	0.006
	Fe-N2	2.1	1.87	7.3		
FePC	Fe-N	4.0	1.99	8.1	8.0	0.013
Fe foil	Fe-Fe	8*	2.47	4.7	5.8	0.001
	Fe-Fe	6*	2.84	5.2	4.1	

(a) N is the coordination number. (b) R is the distance between the absorber and scatterer atoms; (c) σ^2 is Debye–Waller factor to account for thermal and structural disorders; (d)ΔE_0 is inner potential correction.

Table S3 Fe-N bond length information of Fe_{SA}/NSC and Fe_{SA}/NC from DFT calculation and EXAFS fitting.

Sample	Bond type	DFT calculation Bond length (Å)	EXAFS fitting Bond length (Å)
Fe_{SA}/NSC	Fe-N1	1.95	1.98
	Fe-N2	1.87	1.87
Fe_{SA}/NC	Fe-N	1.89	-

Table S4 Elemental contents of C, O, S, N and Fe based on XPS analysis for the catalysts.

Sample	Chemical composition (at%)				
	C	O	S	N	Fe
Fe_{SA}/NSC	84.95	5.21	1.42	8.00	0.42
Fe/NSC-TO	83.22	7.73	1.28	7.32	0.45
Fe/NC-UI	88.73	5.78	-	4.97	0.52
Fe/NC	91.22	5.73	-	2.30	0.75
NSC	87.65	4.75	1.36	6.24	-
NC	92.58	5.91	-	1.51	-

Table S5 Fe contents of Fe_{SA}/NSC, Fe/NSC-TO, Fe/NC-UI and Fe/NC catalysts measured by ICP, wt%.

Catalysts	Fe content (measured by ICP, wt%)
Fe_{SA}/NSC	1.22
Fe/NSC-TO	1.35
Fe/NC-UI	1.06
Fe/NC	1.29

Table S6 Comparison of ORR performance of Fe_{SA}/NSC and other non-precious M−N/C, metal free catalysts, precious metal single atom catalysts from the recent literature and this work (1600 rpm)

Catalysts	Onset potential (V vs. RHE)	Half-wave potential (V vs. RHE)	Media	Reference
Fe_{SA}/NSC	1.03	0.91	0.1 M KOH	**This work**
	0.89	0.77	0.1 M $HClO_4$	
Fe_{SA}/NC	1.00	0.89	0.1 M KOH	Angew. Chem. Int. Ed. 2018, 57, 1-6
	0.94	0.84	0.1 M $HClO_4$	
Fe-ISA/SNC	0.99	0.896	0.1 M KOH	Adv. Mater. 2018, 30, 1800588
	∼0.85	not mention	0.5 M H_2SO_4	
Fe-SAs/NSC	1.00	0.87	0.1 M KOH	J. Am. Chem. Soc., 2019, 141, 20118-20126
	∼0.84	∼0.70	0.5 M H_2SO_4	
Fe-N/P-C-700	0.941	0.87	0.1 M KOH	J. Am. Chem. Soc., 2020, 142, 2404-2412
	0.89	0.72	0.1 M $HClO_4$	
Fe/SNC	not mention	∼0.86	0.1 M KOH	Angew. Chem. Int. Ed., 56, 13800-13804
	not mention	0.77	0.1 M $HClO_4$	
3D MPC Fe-N-C	0.98	0.88	0.1 M KOH	ACS Catal., 2017, 7, 6144-6149
	0.85	0.75	0.1 M $HClO_4$	
Co–N/CNFs	0.92	0.82	0.1 M KOH	ACS Catal., 2017, 7, 6864-6871
	0.82	0.70	0.1 M $HClO_4$	
Zn/NC	not mention	0.873	0.1 M KOH	Angew. Chem. Int. Ed., 2019, 58, 7035-7039
	not mention	0.746	0.1 M $HClO_4$	
S_1N_6C900 carbon nanosheet	0.95	0.83	0.1 M KOH	ACS Appl. Mater. Inter., 2017, 9, 398-405
	0.785	0.47	0.5 M H_2SO_4	

N-HC@G-900	1.0	0.85	0.1 M KOH	Angew. Chem. Int. Ed., 2018, 57, 16511-16515
	0.80	0.65	0.5 M H_2SO_4	
Pt_1@Pt/NBP	-	-	0.1 M KOH	ACS Catal. 2021, 11, 466−475
	∼0.98	0.867	0.1 M $HClO_4$	
Ru-G-750	-	-	0.1 M KOH	Acs Nano 2017, 11, 6930-6941
	0.89	0.75	0.1 M $HClO_4$	
PtFeNC SACs	∼1.02	0.895	0.1 M KOH	Appl. Catal. B-Environ. 2021, 286 119891
	-	-	0.1 M HClO	

1. Z. Lu, B. Wang, Y. Hu, W. Liu, Y. Zhao, R. Yang, Z. Li, J. Luo, B. Chi, Z. Jiang, M. Li, S. Mu, S. Liao, J. Zhang and X. Sun, *Angew. Chem. Int. Ed.*, 2019, **58**, 2622-2626.